JOURNAL OF THERMOPHYSICS AND HEAT TRANSFER
Vol. 23, No. 4, October–December 2009

Cryogenic Heat Pipe for Cooling High-Temperature Superconducting Coils

Daniel W. Kwon* and Raymond J. Sedwick†
University of Maryland, College Park, Maryland 20742

DOI: 10.2514/1.43728

An emerging method of propellantless formation flight is the use of electromagnets coupled with reaction wheels called electromagnetic formation flight. To create a large magnetic field necessary for actuating formation-flying spacecraft, electromagnetic formation flight uses high-temperature superconducting wire. To achieve superconductivity, the high-temperature superconducting wire requires a consumable-free cryogenic thermal control system to maintain the wire temperature below the critical temperature throughout the entire electromagnetic formation-flight coil, which could be as large as 2 m in diameter. The research in this paper investigates a consumable-free method of maintaining isothermalization for a large-scale high-temperature superconducting coil. The high-temperature superconducting coil resides inside a thermally conductive jacket that is used for isothermalization. Both a solid conductor and a heat pipe were investigated for use as the thermally conductive jacket. In this paper, a proof-of-concept circular cryogenic heat pipe was tested in a 2-m-diam toroidal vacuum chamber. This system showed the potential for high-temperature superconducting cooling. The experiments in this paper demonstrate the feasibility of operating large high-temperature superconducting coils for future formation-flying missions.

I. Introduction

AN INCREASING number of missions are considering multiple spacecraft flying in close proximity to replace traditional large monolithic space systems. Examples include formation-flying space interferometers such as NASA's Terrestrial Planet Finder Interferometer [1], ESA's Darwin mission [2], and fractionated spacecraft designs developed by Brown and Eremenko [3]. One of the challenges for formation-flying systems is that the amount of propellant available puts a constraint on mission lifetime and ΔV capabilities. An emerging method of propellantless formation-flight propulsion is the use of electromagnets coupled with reaction wheels. This technique is called electromagnetic formation flight (EMFF). The system is powered by the sun through solar arrays and does not rely on propellant for formation-flying maneuvers. Reducing a satellite's dependence on propellant can change current design methods for future spacecraft formations. For example, the amount of propellant required is currently determined using the rocket equation, and the ΔV required for formation flying is typically a parameter used in the calculation. For propellant-based systems, one method of minimizing propellant mass is to reduce the formation-flying ΔV. Because EMFF is propellantless, the rocket equation is not used. Therefore, by using EMFF, the formation-flight propulsion system can be based on the desired formation performance, without any fuel constraints [4]. As a result, EMFF opens up new capabilities for satellite formations that might have had ΔV requirements that were too costly in terms of propellant to even consider before. Another advantage of EMFF over traditional propellant-based thrusters is the elimination of impinging thruster plumes, which can cause ablation of nearby spacecraft surfaces and produce unwanted vibration excitation. Applications of EMFF are not just restricted to station-keeping fractionated spacecraft architectures or maintaining sparse aperture systems. The electromagnetic (EM) coils can be used with multirole functionality, such as power transmission, torque for slew control, or for passive offensive or defensive capabilities in military satellites [5,6].

To implement EMFF, an EM dipole is created by running current through an electromagnetic coil. A conceptual drawing of an EMFF vehicle is shown in Fig. 1. The EM dipole creates coupled forces and torques on nearby satellites that also have at least one EMFF coil. A satellite with three orthogonal coils can create a steerable dipole in three dimensions. Similarly, a set of three orthogonal reaction wheels is necessary to decouple the forces and torques in three dimensions. Consequently, the EM coils in concert with reaction wheels allow for all the necessary actuation in relative degrees of freedom for a formation-flight array [7]. To create a large magnetic moment to generate large forces, coils that can carry a large current and are large in size are favorable for EMFF.

The high-temperature superconducting (HTS) wire is an enabling technology for EMFF because it allows the creation of a large dipole moment. One of the challenges of using HTS is maintaining the cold temperature necessary for operation. The entire length of the superconducting wire must be maintained below a critical temperature for it to operate at superconducting levels. Commercial off-the-shelf (COTS) wire from American Superconductor Corporation has a critical temperature T_{critical} of 110 K [‡]. For EMFF satellites in the proximity of Earth, such as low Earth orbit (LEO) or geosynchronous Earth orbit, heat flux from the sun and Earth needs to be rejected To maintain temperatures below T_{critical}. This heat flux has the potential to rapidly change in both magnitude and direction, depending on the satellites' orientation. Heat into the coils can be rejected using cryocoolers and various types of insulation such as multilayer insulation (MLI). One characteristic of the HTS wire is that more current can be driven through the wires at colder temperatures, creating a larger dipole field and thus improving the performance of EMFF. However, this benefit comes at the expense of additional power and mass required by the thermal system. In addition to this coupled behavior, the thermal system must also be consumable-free, because EMFF obviates the need for consumables for formation-flying maneuvers. The EMFF thermal system is a unique problem in the topic of cooling large space structures without the use of consumables.

Received 9 February 2009; revision received 15 April 2009; accepted for publication 15 April 2009.

*Faculty Research Assistant, Department of Aerospace Engineering, 3181 Martin Hall. Member AIAA.

†Assistant Professor, Department of Aerospace Engineering, 3181 Martin Hall. Member AIAA.

‡Data available online at http://www.amsuper.com/ [retrieved 2 February 2007].

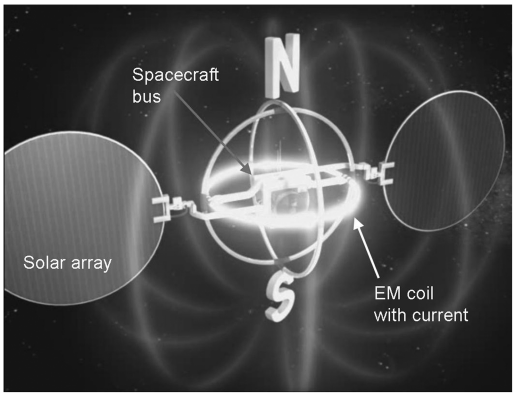

Fig. 1 Conceptual drawing of an EMFF vehicle.

EMFF is not the only application that requires cooling of superconductors in space. Superconducting materials in electric thrusters has been investigated by Bruno and Casali [8]. Other applications include the Variable Specific Impulse Magnetoplasma Rocket (VASIMR) system, which uses HTS coils as a magnetic nozzle [9], and Hoffman and Batishchev [10] proposed using superconducting magnets to create a protective magnetic shield for astronaut radiation protection. All of these systems could benefit from a consumable-free HTS cooling system.

II. EMFF Thermal System

The research in this paper investigates a renewable method of cooling large space structures, such as the HTS coils used for EMFF, which can maintain uniform cryogenic temperatures across large one-dimensional structures operating in orbits in which the thermal environment is characterized by time-varying sources with substantial heat flux, such as Earth infrared and solar reflection and eclipse. There are three challenges of this problem that are important.

First, a renewable method of cooling means that the thermal design must not be reliant on consumables, such as onboard cryogens. Both the method of extracting heat from the system and the distribution of heat should be consumable-free. On the ground, HTS coils are commonly immersed in a bath of liquid nitrogen to maintain a continuous temperature of 77 K. Liquid nitrogen is used on an EMFF ground testbed developed at the Massachusetts Institute of Technology (MIT) Space Systems Laboratory (MIT-SSL), because it operates in a room-temperature, one-atmosphere environment in which conduction and gravity-induced convection make thermal control a challenge [11]. EMFF in LEO will face a high thermal flux environment, but the vacuum allows for other thermal management techniques such as MLI, heat pipes, and cryocoolers. More important, the use of liquid nitrogen on the ground is not traceable to a flight design, because the liquid nitrogen is a consumable. Because one of the benefits of EMFF is to replace consumables, the design of the thermal system must be self-contained. An active cooling system, such as a cryocooler, powered by solar arrays meets the requirements for a heat extraction method.

The second challenge of the problem is the scale of the thermal design, because the HTS coils potentially can be as large as 2 m in diameter [4]. This eliminates devices intended for cooling concentrated point heat sources, such as detectors on space telescopes, and focuses the problem on distributed cooling techniques. It is important to maintain isothermalization of the coil, meaning that minimal temperature gradients exist across the entire coil, because the warmest point in the coil will limit the performance of the HTS wire.

The third challenge of keeping the EMFF HTS coils at cryogenic temperatures is the constantly changing heating environment in Earth orbit. Because of the rapidly changing orientation of the vehicles, heat from the Earth and sun is not constant with respect to time or direction. For this reason, sun shields are not practical for EMFF.

For a flight EMFF thermal system, a cryocooler can be used for heat extraction and MLI can be used to reduce the heat load into the coil, as shown in Fig. 2. One of the first design trades in implementing the HTS coil is to determine if a structure enclosing the wire is required. The MIT-SSL EMFF testbed encloses the HTS coil in a copper containment system or copper jacket, which serves as both a structure enclosing the HTS wire and as a dewar for the cryogen. Therefore, the testbed copper jacket has both structural and thermal functionality. For a flight system, a thermally conductive jacket (TCJ) is defined as the device that functions as both structure for the coil and as a means for the HTS coil to maintain isothermalization. There are two options for enclosing the coil to maintain isothermalization. The first is enclosing the wire inside a solid conductor, by which conduction throughout the coil maintains isothermal conditions. The second option is to enclose the coil inside a solid conductor with a working fluid to maintain isothermalization. An example of the second option is a heat pipe. The research in this paper compares the performance of a cryogenic heat pipe with other consumable-free designs such as a solid conductor as a means for maintaining isothermalization.

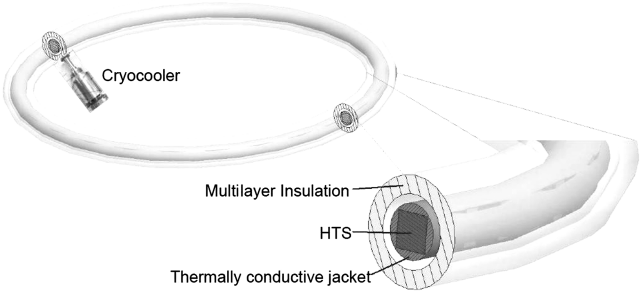

Fig. 2 Design of EMFF HTS coil thermal system with a single cryocooler.

To accomplish the research objective, the first task is to understand the scale of the thermal problem by developing simulation models. Insight can be gained by modeling a solid conductor with and without MLI to determine temperature performance of a system without working fluid, the effect of insulation, and the amount of heat into the system. To gain confidence in the simulation models, experimental testing is conducted. Also, testing in a vacuum chamber environment that has a heat flux greater than low Earth orbit gives confidence that the system will work in space. Next, to determine the benefits of operating a system with working fluid, a heat pipe is investigated. In previous research by Kwon and Sedwick [12], a proof-of-concept straight heat pipe was built to verify modeling and develop the manufacturing process. In this system, HTS wire was inserted into the straight heat pipe to demonstrate the ability of the thermal design to cool HTS. Building from the straight-heat-pipe design, in this paper, a circular heat pipe is designed and built to demonstrate the ability to cool a large-scale HTS coil. As a result, once the cooling methods, heat distribution, and heat rejection methods are modeled and experimentally verified, the thermal design can be migrated to a flight version with high confidence.

One of the unique aspects of an EMFF heat pipe is that the HTS wire resides inside the vapor space of the pipe. Objects that are cooled by heat pipes are typically external to the heat pipe and are in direct contact with the heat-pipe evaporator. This creates a well-defined area for the evaporator in which a large amount of heat is absorbed by the heat pipe. In contrast to this concentrated area of heat into the pipe, the remaining distance along the heat pipe toward the condenser can be modeled as an adiabatic region. For an EMFF coil in space, the distribution of heat depends on its orientation with the sun and Earth. The maximum amount of heat that the coil absorbs occurs when one side is facing the sun and the opposite side is facing the Earth. Here, the entire coil is absorbing heat. The EMFF heat pipe must be designed for this scenario when heat is uniformly absorbed across the entire coil from the external environment. Because the wires in a stack consist of individual strands, providing a small gap between each turn would allow vapor circulation at multiple points along the wire stack.

III. Solid Conductor Case

A. Copper Thermally Conductive Jacket

This section reviews the design for a thermally conductive jacket that relies solely on conduction for isothermalization of the entire coil. No working fluid is used and the system is essentially a heat pipe without working fluid. A finite difference model (FDM) based on the work of Jaluria and Torrance [13] was used to investigate the temperature around the thermally conductive jacket. For a 1-D model, the temperature at each finite difference location i can be determined at every time step $n+1$ by

$$T_i^{n+1} = (T_{i-1}^n - 2T_i^n + T_{i+1}^n)\frac{\alpha \Delta t}{(\Delta x)^2} + \dot{q}\frac{\Delta t}{\rho c} + T_i^n \tag{1}$$

given the time-step duration Δt, properties of the grid, and the thermal diffusivity of the material (α). The TCJ is cooled by a single cryocooler at one location, which is $x = 0$ in this case. For experiments in this paper, the function of the cryocooler is mimicked by a liquid-nitrogen cooling system, which is discussed later. The entire length of the jacket absorbs radiative heat flux from the chamber walls and the surface area of the jacket that experiences the radiation is A_c. The amount of heat flux is a function of the wall temperature T_w. The volumetric heating term is given by the following piecewise function as

$$\dot{q} = \begin{cases} \frac{q_{\text{cryo}}}{\text{volume element}}, & x = 0 \\ \frac{\varepsilon_t \sigma [T_w^4 - (T_i^n)^4] A_c}{\text{volume}}, & x > 0 \end{cases} \tag{2}$$

The volume element has a size equal to $t \cdot 2\pi r_c \cdot \Delta x$ and the entire volume has a size $t \cdot A_c$, where t is the thickness of the pipe. The amount of heat extracted by the cryocooler or liquid-nitrogen cooling system is given by q_{cryo}. The FDM uses the effective emissivity ε_t of the chamber environment, which is a function of the chamber wall properties ε_w and A_w and the pipe properties ε_c and A_c and is given by

$$\varepsilon_t = 1 \Big/ \left[\frac{1}{\varepsilon_c} + \frac{A_c}{A_w}\left(\frac{1}{\varepsilon_w} - 1\right)\right] \tag{3}$$

For comparison with the FDM, a simple 1-D model was simulated using a commercially available thermal code called SINDA/G [14]. As a testing facility for the thermal design, a toroidal vacuum chamber was designed and built by MIT and Aurora Flight Sciences and is shown later. The vacuum chamber, constructed out of COTS polyvinyl chloride tubes, has a major radius of 1 m and a minor radius of 12.5 cm. A Pfeiffer Vacuum Duo 10M rotary vane pump and a Pfeiffer Vacuum TMH 261 turbopump are used to hold a high vacuum (10^{-5} torr).

A copper pipe is used as the test article to represent the thermally conductive jacket. A liquid-nitrogen feedthrough enters the chamber and wraps around the copper pipe so that conduction with the liquid-nitrogen (LN2) tubing provides cooling for the entire copper pipe and acts as the cryocooler. Three carbon fiber G10 rods support the copper pipe to keep it centered in the chamber. The G10 has a low thermal conductivity (0.6 W/m · K at 295 K) to minimize heat conduction to the copper from the walls [15]. Several experiments have been conducted under repeatable conditions, yielding consistent data. A single 250 liter dewar of liquid nitrogen allows for approximately 3 h of cooling time.

The approximate steady-state temperatures throughout the TCJ are shown in Fig. 3a for the measured temperatures (+ marks) and the FDM (solid line). Using the temperature data, the effective emissivity that minimized the mean square error between the measured data and the finite difference model was determined. In Fig. 3 this resulted in an effective emissivity of $\varepsilon_t = 0.2$. To determine how much heat a cryocooler is required to extract, the total absorbed heat flux due to the wall radiation on the coil, Fourier's law is used by the FDM. The thermal load that is extracted by the liquid-nitrogen loops is shown in Fig. 3b and is approximately 25 W in steady state. The transient temperature data are shown later.

The finite difference model matched all the experimental data to within 10 K at the end of the data run (approximately 2.5 h). The time-varying discrepancies between the model and the data are potentially due to the film layer formed in the liquid-nitrogen cooling loops, which gives unsteady cooling. Heat introduction from the G10 spacers holding up the copper pipe and any heat through the thermocouple wires were not incorporated in the model.

The important result is not the fidelity of the model and its comparison with the experiment, but that it was experimentally confirmed that a solid conductor does not allow for isothermalization of the coil. One possible solution is to use multilayer insulation around the copper to reduce the heat load. This is investigated in the next section. The second useful result is that the chamber environment has been modeled and a method of finding the effective emissivity has been determined.

B. MLI Tests

Because tests with the copper TCJ indicate that the temperature gradient is too high to support an entire HTS coil at superconducting temperatures, MLI was wrapped around the copper TCJ to reduce the heat load. This system is shown in Fig. 4. Sheets of Mylar that were 56×84 in. were obtained from Edmund Scientific (part number 3053604). Approximately five total sheets were used wrap the entire coil. The MLI was crinkled by hand so that conduction between layers was minimized. A single sheet allowed for approximately

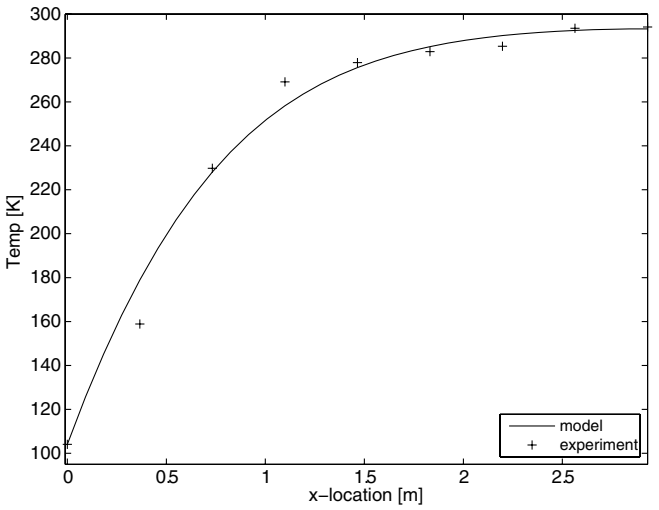

a) Temperature vs distance from LN2 cooling loops

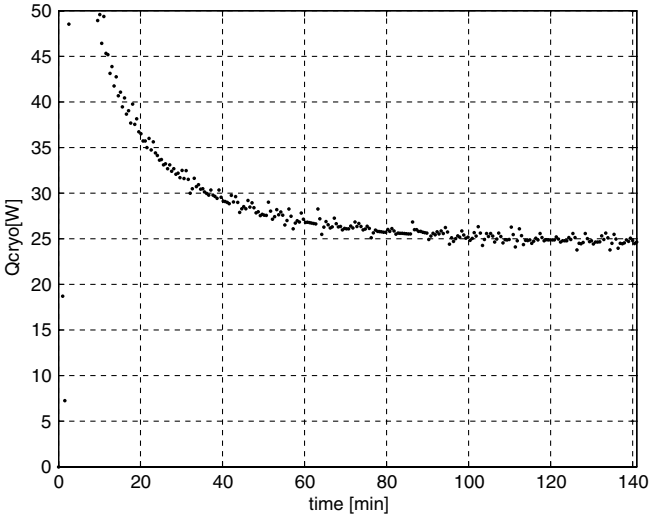

b) Thermal load of TCJ vs time

Fig. 3 Temperature and thermal load of TCJ.

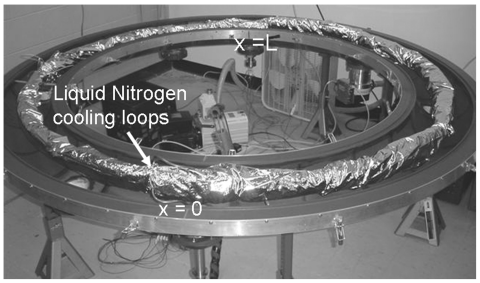

Fig. 4 Copper jacket wrapped in MLI.

seven layers, which were loosely wrapped around the copper pipe. Neighboring Mylar sheets were overlapped to avoid any gaps in MLI coverage. The thermocouples from the previous tests were still bonded to the copper pipe and the wire leads were carefully taken out through small gaps in neighboring sheets at one location. Before testing, the vacuum chamber was pumped down overnight to allow air between the layers to escape.

Tests with the MLI followed the same procedure as for the copper pipe tests, and the results of a representative test are shown in Fig. 5. Tests with MLI took longer to reach an approximate steady-state temperature, because the MLI insulates the copper pipe from changes in temperature. The transient temperature data are shown later, because the data used to estimate the effect of MLI are the temperature at the end of the test (Fig. 5a). From the approximate steady-state temperature, the effective emissivity using MLI was determined to be 0.021, which is a reduction of almost 1 order of magnitude. The MLI also significantly reduced the heat load to approximately 8 W, as shown in Fig. 5b. Compared with the 25 W heat load without the MLI, this is a reduction of approximately 70%. Simulation models for a flight EMFF system in space show that an insulation system capable of reducing the heat load on the order of 80% would be beneficial for a flight design [12]. The MLI used in this paper was close to demonstrating this capability. The 10% difference in heat load between the MLI used in the experiment and the desired MLI performance could be achieved by using more layers of MLI. However, even though the heat load is reduced, the temperature is still greater than T_{critical} throughout most of the coil. Therefore, the next step is to investigate the use of a copper pipe as the TCJ with a working fluid to provide isothermalization of the coil.

IV. Heat Pipe

To bring the state of the EMFF thermal system closer to flight, a circular heat pipe has been designed and tested. A straight heat pipe was demonstrated by Kwon and Sedwick [12] to cool the HTS wire, and the circular heat pipe designed is based on this system. One characteristic about the circular heat pipe is that the system really functions as two heat pipes that share a common condenser and are connected at the far ends of the evaporator. Each heat pipe is half of the coil. They also share the same vapor space, because the HTS wire is continuous inside the heat pipe. For simplicity, the entire coil will be referred to as simply a heat pipe; however, it is important to note that the entire heat load that the coil must carry is actually split between the two pipes. Therefore, if the entire coil must carry 100 W, then half of the coil is simply designed to carry 50 W.

A. Modeling the Circular Heat Pipe

The first step to designing the circular heat pipe is determining the power requirements. Because the pipe is tested inside a vacuum chamber, the heat due to radiation from the chamber walls must be determined:

$$Q_{\text{chamber}} = \varepsilon_t \sigma [T_w^4 - (T_{\text{pipe}})^4] A_{\text{pipe}} \tag{4}$$

The finite difference model for the copper TCJ and chamber environment is used and compared with temperature data. The experimental measurements are for a heat pipe without working fluid inside the vacuum chamber. The heat pipe without working fluid acts just like the copper jacket that was modeled and tested earlier.

Using data for the temperature along the coil, ε_t, the effective emissivity of the pipe and chamber walls can be determined. Figure 6 illustrates the temperature distribution of the coil as a function of axial distance away from the pipe condenser. Again, it is important to note that no working fluid is inside the heat pipe; the condenser was only used to model a cryocooler cooling the pipe at a single location. Figure 6 shows the finite difference model for an effective emissivity of 0.2 (dotted line), 0.3 (solid line), and 0.4 (dashed line). The temperature is measured at various locations, approximately every 36 cm, and is indicated by + marks. The system tested is the fully constructed heat pipe without working fluid. The results show there is an effective emissivity of approximately $\varepsilon_t = 0.3$. The effective emissivity is slightly different from the previous copper TCJ, because of the polish of the circular heat pipe. Now the heat into an operating heat pipe can be determined using the radiation equation, assuming that the entire pipe is at or near saturation conditions. The heat due to the chamber environment is found to be approximately 96 W and is the minimum power capacity that the heat pipe is required to carry.

Modeling for the heat-pipe power capacity using a stainless steel mesh-wicking structure was based on Reay and Kew [16] and Faghri [17]. Given the heat from the environment, the requirement on the

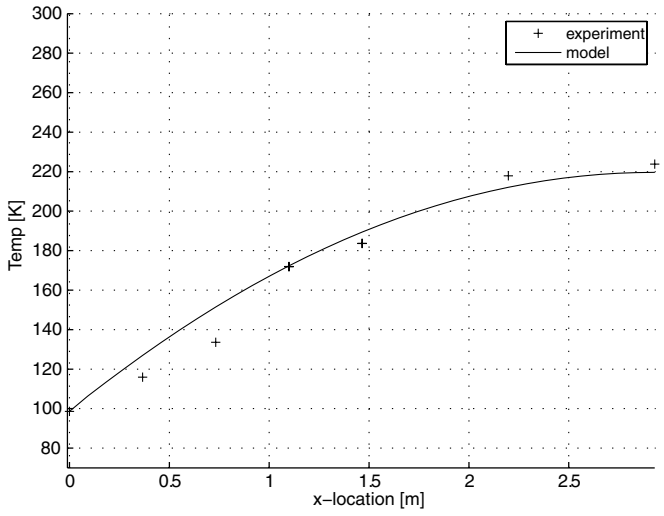

a) Temperature vs distance from LN2 cooling loops

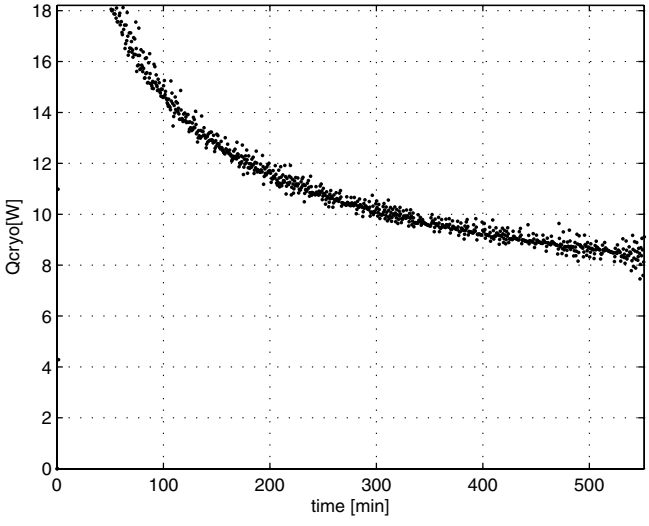

b) Thermal load of TCJ vs time

Fig. 5 Temperature and thermal load of TCJ with MLI.

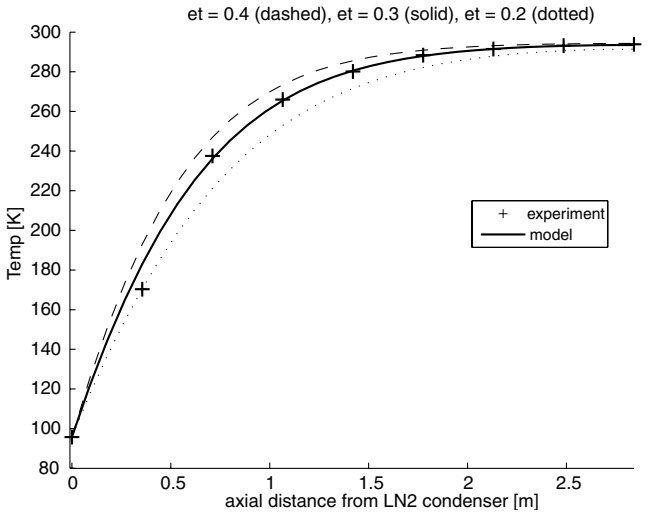

Fig. 6 Temperature vs distance away from the condenser for heat pipe without working fluid.

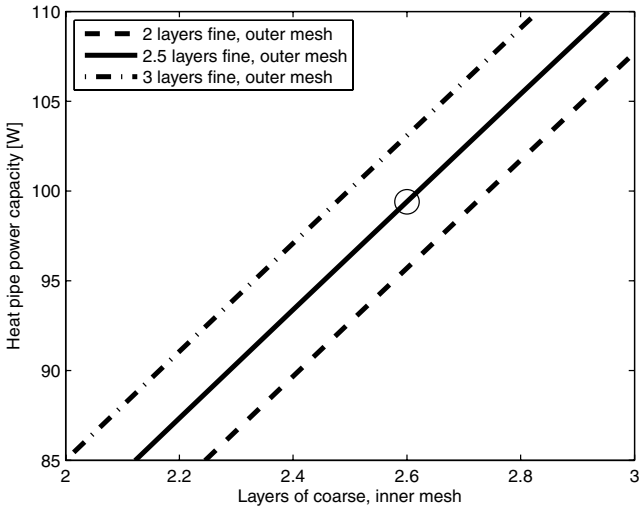

Fig. 8 Heat pipe power capacity of various numbers of inner mesh and outer mesh layers.

minimum heat-pipe power capacity is known. Nitrogen has been selected as the working fluid because its saturation conditions are below T_{critical} and it is a low-cost, safe option compared with other possible cryogenic working fluids. The effective length of the heat pipe is determined by the desired size of the EMFF coil. Flight-sized EMFF coils for a large mission, such as NASA's Terrestrial Planet Finder Interferometer, could be on the order of 2 m in diameter [5]. Because the heat-pipe length is really half of the coil, a heat pipe with a length of 2.84 m was built. This is the distance from the end of the condenser to the halfway point of the coil and does not include the condenser length. Manufacturability of the condenser resulted in a condenser of approximately 17 cm. The total length of the heat pipe plus condenser resulted in a system with a major diameter close to 2 m. The diameter of the pipe's cross section affects the area of the wick. A pipe diameter of 4 cm was sized so that approximately 100 turns of HTS wire could reside inside the pipe, assuming that a minimal area was taken up by a wicking structure.

The wick characteristics are the next parameters to determine, to find the maximum heat-pipe power capacity. Multiple types of stainless steel mesh were used, in which a coarse mesh is located between the pipe wall and the fine mesh. The fine mesh provides favorable capillary pumping pressure, whereas the coarse mesh allows for high liquid-transport ability. A cross-sectional view of this configuration is shown in Fig. 7. Also included in Fig. 7 is a notional configuration for the HTS wire stack. Other types of wick configurations, such as copper sintered wicks [18] or axially grooved heat pipes [19], are potentially more attractive in terms of capillary pressure head or compactness. However, for a proof-of-concept circular-heat-pipe testbed, the stainless steel mesh-wick configuration allows for easier manufacturability and sufficient heat transport ability. Future optimization of the wick in terms of mass, size, and heat transport ability are important considerations for future flight systems.

Using a fine outer mesh with mesh number 250 and a coarse mesh with mesh number 40, the heat-pipe power as a function of the number of mesh layers, for both inner and outer meshes, are shown in Fig. 8. The reason for showing the effects of a various number of

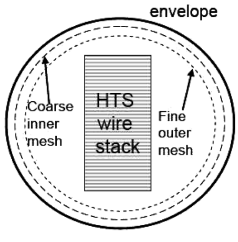

Fig. 7 Cross-sectional cut of heat pipe.

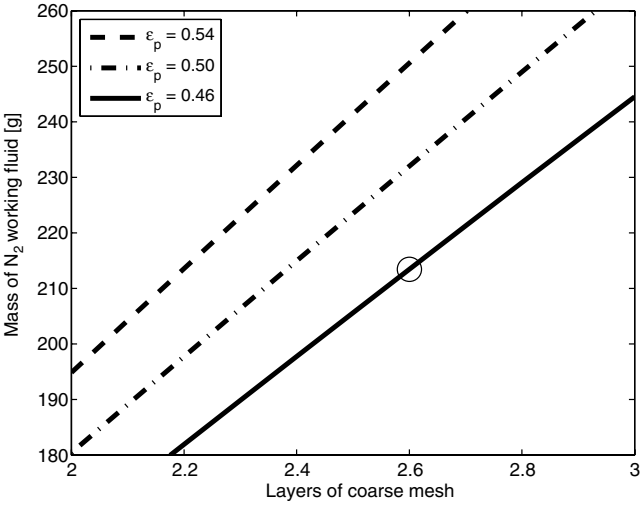

Fig. 9 Working fluid mass.

mesh layers is that implementation of the heat pipe can cause some uncertainty in the effective number of mesh layers present. The heat pipe was designed for a power capacity of approximately 100 W. This corresponds to a heat pipe with approximately 2.5 layers of fine mesh and 2.6 layers of coarse mesh and is shown by the circle in Fig. 8. Also, the results in Fig. 8 are for a heat pipe in which the condenser is located approximately 0.3 deg above the evaporator. The heat-pipe power capacity is sensitive to the angle of the heat pipe. Although the heat pipe was implemented to be as level as possible, a slight tilt in the heat pipe during experimentation was observed.

The amount of working fluid in the coarse mesh was calculated and depends on the porosity ε_p of the wick. The mesh number 40 has a ε_p of 0.54 according to the mesh manufacturer, TWP Inc.[§] However, the working fluid mass varies largely for even small changes in ε_p. Figure 9 shows the working fluid for $\varepsilon_p = 0.54$ (dashed line), $\varepsilon_p = 0.50$ (dashed-dotted line), and $\varepsilon_p = 0.46$ (solid line). The working fluid mass estimated the working fluid mass present in the wick. According to several experimental tests, wick saturation occurred at approximately 210 g of working fluid. Therefore, it is likely that the wick porosity is $\varepsilon_p = 0.46$, as shown by the circle in Fig. 9. A summary of the circular-heat-pipe characteristics is shown in Table 1.

[§]Data available online at http://www.twpinc.com [retrieved 8 August 2008].

Table 1 Summary of EMFF circular heat pipe

Heat pipe length	2.84 m
Pipe diameter	4 cm
Wick material	Stainless steel mesh
Inner mesh layers	2.5 layers of no. 40 mesh
Outer mesh layers	2.6 layers of no. 250 mesh
Condenser length	17 cm
Condenser temperature	~77 K (liquid nitrogen)
Working fluid	Nitrogen
Envelope material	Copper
Approximate power capacity	100 W

B. Testbed Development

Lessons learned from construction of the straight heat pipe [12] were used in construction of the circular heat pipe, including the methods for wrapping the screen mesh and the testing procedures for injecting the working fluid. The differences in constructing a circular heat pipe are that the screen mesh was inserted into a curved section of pipe and the large scale of the circular heat pipe meant individual curved pieces of the pipe envelope had to be cut and then resoldered together. Documentation of these efforts is intended to help bring the Technology Readiness Level of the EMFF coil closer to a brass board state.

Experimental testing of the heat pipe occurs inside a toroidal vacuum chamber, which is shown in Fig. 10 with the top off. The arrows in Fig. 10 indicate the thermocouples on the heat pipe. They are equally distributed throughout the pipe every $L/8$, where L is the distance from the condenser to the end of the evaporator. There are feedthroughs for liquid nitrogen and nitrogen gas and two thermocouple feedthroughs. The heat pipe is supported by three G10 rods, which minimize heat conduction between the pipe and the chamber walls.

Before inserting the screen, both the pipe and the screen were cleaned in multiple acid baths to eliminate any contaminants, grease, and oxidation. The procedure for screen and pipe cleaning is outlined by Peterson [20]. An HTS wire was not inserted into the circular heat pipe, because cooling of HTS wires was already validated in the straight-heat-pipe tests [12]. In the straight-heat-pipe system, the electrical feedthroughs connecting the HTS wire caused the heat pipe to leak. To minimize complications caused by leaking working fluid, the HTS wire was not inserted. The goal to demonstrate the ability to cool large-scale HTS coils can still be achieved with this circular EMFF heat pipe.

One of the main challenges to constructing the circular heat pipe was inserting the screen mesh. For the screen mesh to maintain good capillary pressure throughout the entire length of the pipe (half of the coil), a continuous piece of mesh is desired. The mesh required a length around 3 m to account for margin; however, the mesh was manufactured in smaller lengths. To create a longer continuous piece, the mesh was overlapped and soldered together. To minimize interference with the working fluid (both the capillary pressure and the liquid transport), the mesh was overlapped by only 2 to 3 mm, and each overlap contained only four solder joints, each with an area less than 10 mm^2.

A second challenge faced during construction was that the mesh is not very rigid and tends to crumple or fold on itself easily when pushed into a pipe. To help mitigate the situation, the heat pipe was cut into eight separate sections so that each section was approximately 75 cm long. Instead of pushing the screen through half of the coil, the screen only needed to be pushed through a single section. When the screen appeared through the end of a pipe section, the screen was pulled through so that there was enough screen for the neighboring pipe sections. When the screen was inserted into each half of the circular pipe, all the sections were soldered together. The ends of the screens for each half of the pipe are located at the middle of the condenser, where the two halves meet at the end of the evaporator, 180 deg away from the condenser.

A liquid-nitrogen reservoir was built to extract heat from the system in place of a cryocooler. This system is shown in Fig. 11. The liquid nitrogen in the reservoir is isolated from the inside of the pipe and is in direct contact with the outside of the pipe, forming a condenser with a length of approximately 17 cm. The reservoir was constructed by soldering wrought solder fittings onto a copper bushing. One end of the bushing is in contact with liquid nitrogen and the opposite end serves as the end of the condenser. Liquid nitrogen enters the bottom of the reservoir, whereas nitrogen gas due to boiloff escapes out of the top of the reservoir. Thermocouples are located at the top, middle, and bottom of the LN2 reservoir to help monitor the liquid level. Nitrogen gas from a gas tank is measured by an Omega FMA 1600A series flowmeter and then enters the vacuum chamber via a gas feedthrough. The working fluid enters the pipe at the end of the evaporator, at location L. Also connected to the heat pipe are a relief valve and a digital pressure gauge. A power resistor is located at L and is used to test the power capacity of the heat pipe.

C. Experimental Results

The testing procedure for the circular heat pipe was similar to the testing procedure for the straight heat pipe. Testing of the EMFF heat pipe begins by flowing liquid nitrogen into the LN2 reservoir. This begins at time $= 0$ min. Initially, the pipe is filled with nitrogen gas at approximately 40 psi. As the pipe starts to cool, pressure inside the pipe decreases. After about 10 min, the LN2 reservoir is full and the working fluid begins to rapidly condense inside the pipe in the region surrounding the condenser. As the pipe pressure continues to drop and condensation occurs, working fluid is injected periodically, approximately every 5 min. Working fluid is injected at pressures between 40 and 45 psi, depending on how much fluid resides in the wick.

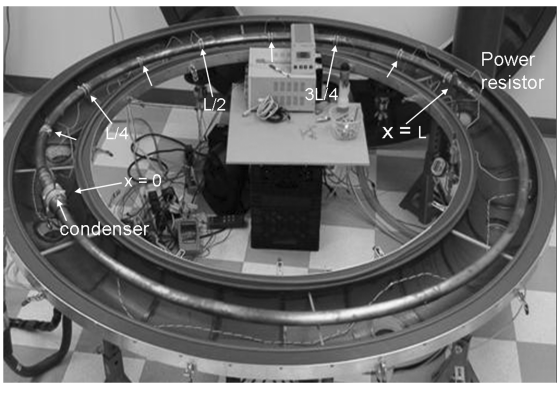

Fig. 10 Toroidal vacuum chamber with heat pipe.

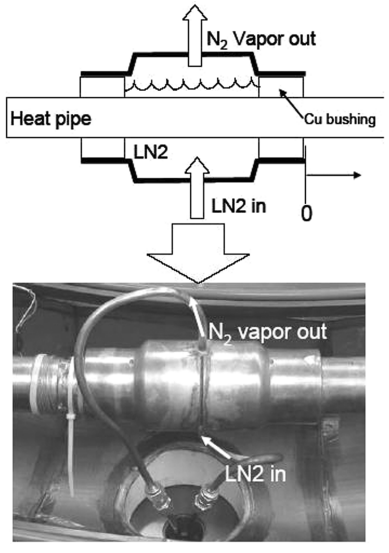

Fig. 11 Liquid nitrogen reservoir for circular heat pipe.

The bottom plot in Fig. 12 illustrates the temperature of the pipe as a function of time. There are 13 thermocouples located inside the chamber. Three are located on the LN2 reservoir, nine are located on the pipe, and one thermocouple measures the chamber wall temperature inside the vacuum. The first thermocouple is located right next to the copper bushing on the pipe and is the $x = 0$ location (see Fig. 11). The length of half of the pipe is L, and each of the remaining thermocouples is spaced at distances $L/8$ apart, which is approximately 36 cm. This is the same thermocouple configuration from Fig. 10. Only the thermocouples located every quarter of the pipe half-length are shown in Fig. 12 for clarity.

The cumulative amount of working fluid in the pipe is shown in the top plot in Fig. 12. Analyses from the previous section and previous tests were conducted to determine the amount of working fluid to wet the entire length of the wick. After approximately 120 min, the wick is wetted and approximately 210 g of working fluid have been injected. Once there is sufficient working fluid in the pipe, the liquid is slowly transported throughout the entire wick and saturation conditions exist throughout the pipe. This occurs around 150 min into the test and the temperature is below the critical temperature for the HTS wire.

The heat pipe is designed to carry heat absorbed from the external environment. Heat absorbed throughout the entire pipe, which is the evaporator drives the circulation of the working fluid inside the pipe. To design for additional heat loads, such as quench or thermal instability, a higher maximum power capacity can be accounted for. To test for higher power inputs, a 50 W power resistor located at the end of the heat-pipe evaporator is used to introduce heat into the system. To test the heat-pipe power capacity and to determine dry-out conditions, a resistor at location L, near the $x = L$ thermocouple, is used as a heating source. The power profile for the resistor is shown in the top plot of Fig. 12. Note that there is also approximately 96 W into the heat pipe due to radiation from the chamber walls.

The pressure in the pipe and in the vacuum chamber is measured. Once the heat pipe has reached saturation at 150 min, the pipe pressure is relatively steady at 42 psi. The pressure seen is consistent with the pressure and temperature for nitrogen at saturation. A pressure of 42 psi corresponds to a temperature of approximately 88 K, according to the nitrogen saturation properties. The vacuum chamber pressure operates between 4 and 6 mbar during testing. The toroidal chamber itself had some leaks in it, independent of the heat pipe. However, operating at these pressures provides a sufficient vacuum for testing.

Introducing additional heat into the system via the power resistor elevates the temperature at the end of the evaporator. This is shown in Fig. 12 by the increased temperature as the thermocouple at the evaporator end (L) rises at around the 180 min mark. When the heat pipe is carrying a total of 111 W, the temperature rises above the wire critical temperature (110 K). Any section of the superconductor that is above the critical temperature does not superconduct and will limit the current of the entire wire. For each resistor power level, the power applied was held until an approximate steady-state condition was observed by the L thermocouple. After power is removed, the heat pipe returns to saturation conditions throughout the pipe at around 290 min into the test. After the test, the heat pipe is vented and the working fluid exiting the pipe is also measured by the flowmeter to double-check the working fluid mass present. This test measured a vented mass of 205.4 g, which has a 1.6% difference with the injected mass and correlates to the accuracy of the flowmeter. No significant amounts of working fluid are observed to be leaked during testing of the circular heat pipe.

The temperature around the heat pipe at various power levels is also shown in Fig. 13. The approximate steady-state temperature at each applied power level (0, 5, 10, and 15 W) used by the resistor was used to generate Fig. 13. Dry-out of the wick occurs when there is a large increase in temperature beyond the saturation conditions and indicates that the maximum heat-pipe power capacity has been exceeded. From Fig. 13, dry-out occurs in the region of large temperature increase when the resistor is set to generate 10 W, meaning that the heat pipe is carrying approximately 106 W total. The experimental results of the heat pipe show a heat-pipe power capacity that is close to the desired design of 100 W, with

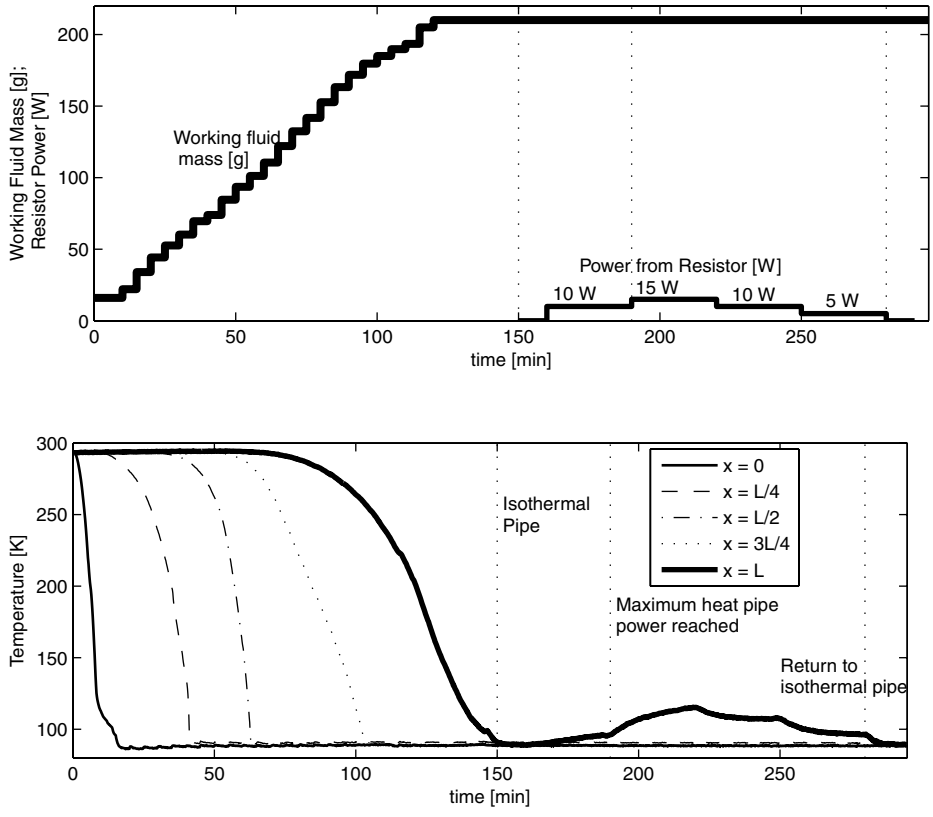

Fig. 12 Testing a circular EMFF heat pipe showing working fluid mass, resistor power and temperature.

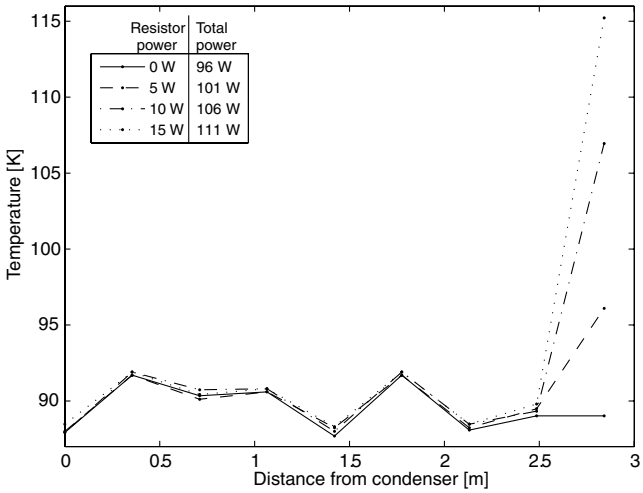

Fig. 13 Temperature around heat pipe for various amounts of power from resistor.

approximately 6% deviation. The overall results show that cooling of large-scale HTS coils can be achieved using a cryogenic heat pipe for isothermalization.

D. HTS Performance

The critical current density I_c of the HTS wire is affected by the operating temperature and the magnetic field across the wire. In a stack of HTS wires, the magnetic field from other wires in the stack act to reduce the maximum current and the resulting magnetic moment. To understand how the magnetic field affects EMFF, the wire stack configuration used for a single coil is investigated. In a separate experimental ground EMFF testbed vehicle [11], a single coil is composed of three neighboring wire stacks, which are separated by approximately 8 mm. The HTS wire used is a Bi-2223 tape with a critical current of 115 A at 77 K with no magnetic field. The testbed vehicles consist of two orthogonal coils, which are bath-cooled by liquid nitrogen. The maximum observed current when both coils are running current is 95 A, which is a reduction in I_c of approximately 17% [5]. This reduction in I_c is primarily due to the magnetic field within a single stack for a coil. The magnetic field from neighboring stacks and other orthogonal coils are a higher-order effect. For a circular-heat-pipe system, the I_c reduction due to operating at a temperature greater than 77 K is approximately 10% [12]. One of the objectives for a future testbed is to reduce the temperature at which isothermalization occurs, to improve the critical current density. The operating temperature of the proof-of-concept circular heat pipe or experimental results from the ground EMFF vehicles indicate that magnetic moment is not a limiting factor for future EMFF systems.

V. Summary of Experiments

The research in this paper has examined the performance of a TCJ as a means of isothermalization for a large-scale HTS coil for EMFF. First, the use of a solid conductor or copper jacket, both with and without MLI, was examined. The copper jacket is essentially a heat pipe without working fluid. Then the use of a heat pipe with working fluid was examined. A summary of the experimental results as a function of time for all three circular thermally conductive jacket systems is shown in Fig. 14. Shown are the transient temperatures for the heat pipe without working fluid (dotted line), the heat pipe without working fluid but with MLI (dashed line), and the heat pipe with working fluid (solid line). For each of the systems, temperature data at locations $x = 0$, $L/8$, $L/4$, $L/2$, and L are given. The efficiency of operating with a working fluid is clearly shown in Fig. 14, and the heat pipe was the only TCJ system that was capable of reaching temperatures below T_{critical}. Here, the efficiency of heat transport ability can be examined by the thermal conductivity of the device carrying heat, either the solid conductor or the heat pipe. Using the experimental data, a conservative estimate for the effective thermal conductivity of the heat pipe with working fluid is 214 kW/m · K. This is a 52,000% improvement over solid copper, which is the heat pipe without working fluid. In general, a benefit of using heat pipes is that there are no moving parts, and so the system has high reliability, which is an important characteristic for integration with spacecraft.

One of the difficulties in comparing the transient temperature data is that not all three tests lasted for the same duration. The test for the heat pipe without working fluid and no MLI lasted for only 145 min, whereas the other two tests lasted beyond 295 min. The heat pipe with working fluid used a resistor to change the heat carried, whereas the other two tests did not. Another aspect that is different is that the condenser or liquid-nitrogen reservoir for the tests without working fluid was built differently from the heat pipe with working fluid. Cooling for the copper jacket systems was composed of loops of copper tubing with liquid nitrogen flowing inside. These loops of copper tubing were in direct contact with the copper jacket. This cooling system had much less thermal mass than the liquid-nitrogen system used for the heat pipe with working fluid. Therefore, the tests without working fluid were able to lower their temperature more rapidly at locations $x = 0$ and $L/8$, compared with the heat pipe with working fluid. However, once enough working fluid is injected and starts to circulate, the temperature of the heat pipe drops significantly and reaches near isothermal conditions once the wick is saturated. The two systems without the working fluid are unable to match these conditions.

Using the approximate steady-state temperature for all three TCJ systems shown in Fig. 14, the temperature as a function of axial distance along the length of the pipe away from the condenser is shown in Fig. 15. For the two TCJ systems without working fluid, the finite difference models (solid lines) are shown along with the experimental data. It should be noted that for the system with MLI, the approximate steady-state experimental data was taken at 550 min, which is not shown in Fig. 14. There are two conclusions that are summarized in Fig. 15. First, the benefits of operating with a working fluid are shown by comparing the heat pipe without working fluid and with working fluid. Both systems were operated in the toroidal vacuum chamber and had relatively similar heat loads. The heat load carried by the heat pipe was higher, due to a difference in the effective emissivity. However, the copper TCJ has a large temperature gradient, whereas the heat pipe with working fluid is able to achieve isothermal conditions below T_{critical}.

Second, the benefits of operating with insulation are shown by comparing the copper TCJ system with and without MLI, because MLI is able to reduce the heat load by approximately 70%. Although the temperature gradient is lower for the MLI case, it is still not

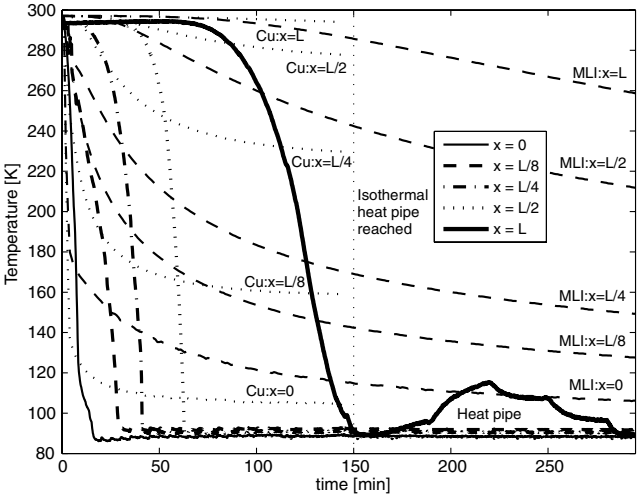

Fig. 14 Transient temperatures for heat pipe with working fluid, heat pipe without working fluid, and heat pipe without working fluid with MLI.

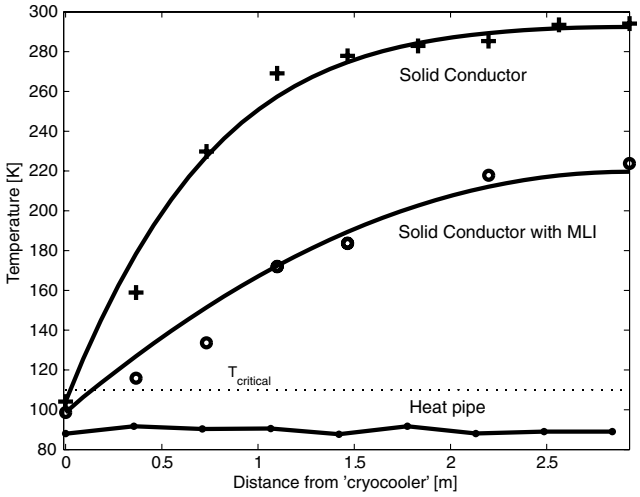

Fig. 15 Temperature vs axial distance from the condenser for heat pipe, heat pipe without working fluid, and heat pipe without working fluid with MLI.

sufficient for operating the HTS. One item for future testing would be to consider using additional MLI to determine how much more the heat load can be reduced. Operating in a thermal vacuum chamber may allow for further reduction of the heat load and simulation of space heating conditions.

VI. Conclusions

Electromagnetic formation flight is a unique and promising propellantless propulsion system for future formation-flying satellites. To implement EMFF, a cryogenic thermal control system is required to cool the high-temperature superconducting coils. A thermal system that is also consumable-free consists of a cryocooler to extract heat and a cryogenic heat pipe to maintain isothermalization of the coils. A thermally conductive jacket surrounds the HTS coil to provide isothermalization and structure for the wire stack. The benefit of enclosing the wire is that thermal gradients across the HTS wire stack can be minimized if the thermal jacket is isothermal. First, the performance of a copper pipe acting as a solid conductor for the thermally conductive jacket was investigated by a finite difference model and experimental testing. A solid conductor was unable to achieve the low temperatures necessary for the HTS coil, even using MLI to reduce the heat load. Therefore, a circular cryogenic heat pipe was designed and built for use as the thermally conductive jacket. The circular heat pipe had a 2 m major diameter and was tested inside a toroidal vacuum chamber. Experimental results show the entire coil reaching saturation condition after sufficient working fluid was injected into the heat pipe. Using the cryogenic heat pipe, this research has demonstrated the feasibility of operating large-scale HTS coils in space without using consumables.

One of the next steps is to test the EMFF thermal system in a thermal vacuum chamber. This system can use multiple radiative heating sources to mimic the effect of the sun and Earth for a satellite in low Earth orbit. This initial test could use the current circular heat pipe with MLI in a thermal vacuum chamber with the walls at liquid-helium temperature. However, a redesigned circular heat pipe that has a power capacity closer to a flight system has more relevance. A next step beyond this is the integration of a cryocooler and use of multiple coils with heat pipes. Testing in a thermal vacuum chamber of at least two separate EMFF coils, each with a complete thermal system, should be conducted to determine the forces and torques achievable during realistic flight conditions. The heat pipe should be initially sealed to determine the startup conditions needed to use the coils. After testing of two separate coils, the use of two testbed vehicles with multiple coils should be considered in the thermal vacuum chamber. The testbed can either use a single cryocooler for each coil or one shared among the coils on each vehicle. In a relevant operating environment, this system would demonstrate high confidence in bringing EMFF satellites to flight.

References

[1] Blackwood, G., Henry, C., Serabyn, E., Dubovitsky, S., Aung, M., and Gunter, S. M., "Technology and Design of an Infrared Interferometer for the Terrestrial Planet Finder," AIAA Space 2003 Conference, AIAA Paper 2003-6329, Long Beach, CA, Sept. 2003.

[2] Cockell, C. S., Leger, A., Fridlund, M., Herbst, T., Kaltenegger, L., and Absil O., "Darwin—A Mission to Detect and Search for Life on Extrasolar Planets," *Astrobiology*, Vol. 9, No. 1, 2009, pp. 1–22. doi:10.1089/ast.2007.0227

[3] Brown, O., and Eremenko, P., "Fractionated Space Architectures: A Vision for Responsive Space," AIAA 4th Responsive Space Conference, AIAA Paper RS4-2006-7506, Washington, D. C., 2006.

[4] Kong, E. M. C., Kwon, D. W., Schweighart, S. A., Elias, L. M., Sedwick, R. J., and Miller, D. W., "Electromagnetic Formation Flight for Multisatellite Arrays," *Journal of Spacecraft and Rockets*, Vol. 41, No. 4, 2004, pp. 659–666. doi:10.2514/1.2172

[5] Kwon, D. W., and Miller, D. W., "Electromagnetic Formation Flight of Satellite Arrays," S.M. Thesis, Space Systems Lab., Rept. 2-05, Massachusetts Inst. of Technology, Cambridge, MA, Jan. 2005.

[6] Gardner, P. G., "A Study of Selected Aspects of Electromagnetic Formation Flight," M.S. Thesis, Univ. of Maryland, College Park, MD, Sept. 2008.

[7] Elias, L. M., Kwon, D. W., Sedwick, R. J., and Miller, D. W., "Electromagnetic Formation Flight Dynamics including Reaction Wheel Gyroscopic Stiffening Effects," *Journal of Guidance, Control, and Dynamics*, Vol. 30, No. 2, 2007, pp. 499–511. doi:10.2514/1.18679

[8] Bruno, C., and Casali, D., "Superconducting Materials Applied to Electric Propulsion Systems," *Journal of Spacecraft and Rockets*, Vol. 41, No. 4, 2004, pp. 671–676. doi:10.2514/1.11938

[9] Schwenterly, S. W., Carter, M. D., Chang-Diaz, F. R., and Squire, J. P., "HTS Magnets for Advanced Magnetoplasma Space Propulsion Applications," *Advances in Cryogenic Engineering*, Vol. 45A, 2000, pp. 603–607.

[10] Hoffman, J., and Batishchev, O., "Use of Superconducting Magnet Technology for Astronaut Radiation Protection," NASA Institute for Advanced Concepts, Atlanta, GA, May 2005.

[11] Neave, M., "Dynamic and Thermal Control of an Electromagnetic Formation Flight Testbed," S.M. Thesis, Space Systems Lab., Rept. 07-05, Massachusetts Inst. of Technology, Cambridge, MA, June 2005.

[12] Kwon, D. W., and Sedwick, R. J., "Cryogenic Heat Pipe for Cooling High Temperature Superconductors with Application to Electromagnetic Formation Flight," Ph.D. Thesis, Space Systems Lab., Rept. 1-09, Massachusetts Inst. of Technology, Cambridge, MA, Feb. 2009.

[13] Jaluria, Y., and Torrance, K. E., *Computational Heat Transfer*, 2nd ed., Taylor and Francis, New York, 2003.

[14] SINDA/G, Software Package, Ver. 2.4, Network Analysis, Inc., Chandler, AZ, Feb. 2005.

[15] Frederking, T. H. K., and Yuan, S. W. K., *Cryogenics—Low Temperature Engineering and Applied Sciences*, Yutopian Enterprises, Santa Monica, CA, 2005.

[16] Reay, D. A., and Kew, P. A., *Heat Pipes*, 5th ed., Elsevier, Boston, 2006.

[17] Faghri, A., *Heat Pipe Science and Technology*, Taylor and Francis, Washington, D.C., 1995.

[18] Peterson, G. P., and Fletcher, L. S., "Effective Thermal Conductivity of Sintered Heat Pipe Wicks," *Journal of Thermophysics and Heat Transfer*, Vol. 1, No. 4, 1987, pp. 343–347. doi:10.2514/3.50

[19] Kobayashi, Y., Syuji, I., Iwasa, M., "Evaporative Heat Transfer at the Evaporative Section of a Grooved Heat Pipe," *Journal of Thermophysics and Heat Transfer*, Vol. 10, No. 1, 1996, pp. 83–89. doi:10.2514/3.756

[20] Peterson, G. P., *An Introduction to Heat Pipes—Modeling, Testing, and Applications*, Wiley, New York, 1994.